Engineering Microbiology 6 (2026) 100249

Contents lists available at ScienceDirect

Engineering Microbiology

journal homepage: https://www.keaipublishing.com/en/journals/engineering-microbiology/

Original Research Article

Analysis of the PRE configuration reveals the constraints in Ste12 oligomerization in mediating pheromone-inducible transcription in *Saccharomyces cerevisiae*

Yiqing Zhang[a,†], Yinfeng Wei[a], Yuxin Huang[a], Chenyu Wang[b], Tao Wang[a], Yujiao Wang[b], Yingxuan Qi[a], Guannan Liu[a,*]

[a] College of Biotechnology and Pharmaceutical Engineering, Nanjing Tech University, Nanjing 211816, China
[b] College of 2011, Nanjing Tech University, Nanjing 211816, China

ARTICLE INFO

Keywords:
Transcription
Pheromone-inducible promoter
PRE configuration
Ste12 oligomerization
DNA looping

ABSTRACT

Yeast cell mating is regulated by the transcription factor Ste12, which activates the transcription of mating genes by binding to pheromone response elements (PREs) in their promoters. PREs vary in number and position among different promoters. However, the effect of PRE organization on Ste12-promoter interactions and the possible downstream transcription of mating genes remains to be fully understood. In this study, we analyzed yeast pheromone-induced gene expression using RNA-seq transcription profiling. We retrieved the promoters of the significantly upregulated genes, focusing on the occurrence and arrangement of PREs. *PPRM1*, which carries three adjacent consensus PREs, was selected as a model for investigating the relative contribution of each PRE to promoter activity through single-base mutation or deletion. We then evaluated the impact of different PRE organizations on pheromone-induced expression by altering their orientations and copy numbers. Subsequently, we proposed a model to explain the mechanism of transcriptional regulation of pheromone-inducible genes, in which the organization of PREs modulates promoter activity by influencing Ste12 oligomerization. This study paves the way for deciphering the transcriptional mechanisms of eukaryotic regulatory systems.

1. Introduction

Cell mating in *Saccharomyces cerevisiae* begins with the sensing of pheromones produced by cells of the opposite mating type [1]. This process involves the mitogen-activated protein kinase (MAPK) signal transduction cascade, leading to the activation of the cell mating-specific transcription factor Ste12 [2–6]. Upon activation, Ste12 binds to pheromone response elements (PREs) in the promoters of over 200 pheromone-responsive genes, activating their transcription [7,8].

PREs are known to contribute to yeast pheromone-inducible expression [9,10], as demonstrated by functional investigations of the promoters of genes such as *PRM1, FUS2, AGA1* [11], and *FIG1* [12]. Consensus PREs carry the conserved sequence motif of 5′-TGAAAC-3′ and function as an enhancer to a heterologous core promoter [12–17]. This element is necessary and sufficient to activate gene expression in response to pheromones [16]. The integrity of the consensus PRE (cPRE) is very important for pheromone-inducible expression, as mutagenesis of the G at position 2 or each of the As at positions 4 and 5 abolishes or strongly reduces the pheromone-inducible expression of engineered promoters [11]. To distinguish them from the fully functional cPRE, we designated mutants at one of the six base positions as non-consensus PREs (ncPREs).

Although it has been reported that there is a large variability in the number, orientation, spacing, and sequences of PREs among all promoters [11,15,18,19], the impact of diverse PRE arrangements on the intrinsic principles between transcription factors and promoter expression levels remains poorly understood. In 2010, Su and colleagues used a heterologous core promoter p*GAL1* assay and reported the effects of orientation ("head-to-head," "tail-to-tail," or tandem) and/or differences in spacing (10, 20, 40 nucleotides), revealing that two PREs interspaced 40 nucleotides apart in either a head-to-head or tail-to-tail orientation conferred strong inducible activity, while the tandem arrangement was inactive [11]. In addition, a single PRE failed to confer pheromone-inducible expression on synthetic promoters derived from the core promoters of p*CYC1* and p*GAL1* [11,12,20]. In contrast, native promoters carrying a single PRE confer pheromone-inducible expression [11]. Further complexities arose from the fact that multiple PREs may operate in a non-additive, cooperative fashion to facilitate pheromone-inducible expression [12], whereas removing the ncPRE from p*CIK1* led to com-

* Corresponding author.
E-mail address: 360265597@njtech.edu.cn (G. Liu).
† Present address: Shenzhen Institute of Advanced Technology, Chinese Academy of Sciences, Shenzhen 518055, China.

https://doi.org/10.1016/j.engmic.2025.100249
Received 6 August 2025; Received in revised form 18 November 2025; Accepted 21 November 2025
Available online 19 December 2025

plete loss of inducibility [11]. Moreover, the inducible activity of these promoter mutants was completely abolished when either the cPRE or adjacent ncPRE within the p*FIG1* nucleosome-unfavorable region was mutated to a non-PRE. Importantly, when an ncPRE was mutated into a cPRE, there was almost no change in the induction activity of the promoter mutant, with only a marginal enhancement observed in the response speed compared with the wild-type [18]. To this end, systematic characterization is required to reveal how multiple PREs cooperate to confer pheromone-inducible expression from the core promoter.

Here, we examined the contribution of proximal cPREs to the activity of the *PRM1* promoter using motif deletions or single-base mutations to abolish the affinity between cPREs and Ste12. Given that the activation of gene expression is modulated by changes in the orientation and copy number of PREs, we further investigated the effects of cPRE orientation and the copy number of PREs on promoter activity. We found that both proximal and distal PREs function as enhancers, and our results further support the hypothesis that PRE-bound Ste12 proteins promote transcription via oligomerization.

2. Materials and Methods

2.1. Strains, plasmids, and growth conditions

The gene expression vector used in this study was based on the plasmid pRS415, which was extracted using the AXYGEN AxyPrep Plasmid Miniprep Kit. After transforming the recombinant plasmids into *Escherichia coli* DH5α, positive clones were obtained on Luria–Bertani medium (LB; 0.5% NaCl, 1% tryptone, 0.5% yeast extract) supplemented with ampicillin (100 μg/mL) at 37°C.

The MATα haploid strain of *S. cerevisiae* (BY4741) was used as a host for promoter engineering in this study. Wild-type yeast cultures were routinely cultured in standard Yeast Peptone Dextrose medium (YPD; 1% w/v yeast extract, 2% w/v peptone, and 2% w/v glucose) at 30°C. For yeast transformation, *S. cerevisiae* BY4741 was plated on synthetic complete (SC) media without the auxotrophic compound.

2.2. Plasmid construction

The primers used in this study are listed in Table S2. The recombinant plasmids contained UAS elements (UAS_{prm1}), core promoters (p*PRM1/FIG1/FUS2/AGA1/TEF2*), yEGFP, and CYC1 terminators. The Gibson assembly technique was used to assemble these fragments, using pRS415 as the expression vector backbone. The assembled products were then transformed into *E. coli* DH5α for amplification. After yeast transformation, colonies were selected on SC-Leu dropout plates and confirmed using colony PCR for subsequent experiments. Primer synthesis and DNA sequencing services were provided by GENEWIZ Inc. (Suzhou, China).

2.3. Transcriptome sequencing

Wild-type BY4741 was incubated in YPD medium at 30°C, 200 rpm for 24 h. The seed culture was then diluted to 50 mL with fresh medium to a final OD_{600} of 0.1. After 5 h of growth, the cells were induced for 0, 20, and 40 min with 5 μM α-pheromone. The cells were harvested via centrifugation at 3000 ×*g* for 5 min at 4 °C, and then the cell pellets were stored in TRIzol at –80°C. Three replicates from each group were sent to Shanghai Majorbio Bio-Pharm Technology for RNA extraction and sequencing.

2.3.1. Validation of RNA-Seq using quantitative PCR

To verify the accuracy of the transcriptome results, qPCR was performed at the mRNA level. When yeast cultures reached a final OD_{600} of 0.6, the cells were treated with pheromones (GenScript) for 0, 20, or 40 min. RNA was extracted via zymolyase digestion of the yeast cell wall using a FastPure Cell/Tissue Total RNA Isolation Kit (Vazyme) according to the manufacturer's instructions. The total cDNA was synthesized from purified RNA (ranging from 1 pg to 1 μg) using a HiScript III RT SuperMix for qPCR (+gDNA wiper) from Vazyme. cDNA (100 ng) was used for qPCR. The primers for qPCR were designed using the NCBI website and synthesized by GENEWIZ (Appendix Table S2). Quantitative PCR was performed using the ChamQ Universal SYBR qPCR Master Mix (Vazyme) on a StepOne Real-Time PCR System (Thermo Fisher Scientific). The thermocycling conditions were set as follows: predenaturation at 95°C for 3 min, followed by 40 cycles of denaturation at 95°C for 10 s and annealing at 60°C for 35 s. Relative transcript levels were represented as the expression level of the target gene divided by that of *tdh1*, which served as the reference gene [21].

2.4. Flow cytometry

To characterize the strength of the yeast pheromone-responsive promoter, the fluorescence intensity of the transformants was measured using flow cytometry. Single colonies of the constructed strains were grown in 5 mL of fresh SC-Leu medium for 24 h. Then, the seed culture was diluted to an OD_{600} of 0.1 with 50 mL of SC-Leu medium, and continued shaking was performed at 30°C, 220 rpm for 3 h. Cells were treated with 5 μM of α-pheromone for one hour. After centrifugation, the cell pellet was washed twice with 1 M phosphate-buffered saline (PBS) and resuspended in 2 mL PBS. For flow cytometric analysis, 200 μL of the yeast culture were transferred into a 96-well microplate to analyze GFP expression by measuring the fluorescence intensity using a BD FACS Aria III (BD Biosciences) or Beckman Coulter CytoFLEX. GFP was excited using a 488 nm laser and detected through a 530/20 nm bandpass filter (FL1.A), with 10,000 events recorded per sample. All data were analyzed using FlowJo™ software. Because fluorescence intensity represents relative values rather than absolute values, it should not be compared across different experimental batches. Instead, we focused on the relative changes in p*PRM1* or other engineered promoters with or without inducers, defined as the fold induction.

2.5. Statistical analysis

Data analysis and visualization were performed using GraphPad Prism 8.4. All experiments were performed in triplicate, and statistical significance was assessed using one-way ANOVA. Data are expressed as the mean ± standard error of the mean.

2.6. Nucleosome position prediction

Nucleosome positions were predicted using the NuPoP Nucleosome Positioning Prediction Engine (http://nucleosome.stats.northwestern.edu/) [22]. The output file includes five columns: position, P-start, occupancy, N/L, and affinity. Occupancy defines the possibility that a given position is covered by a nucleosome, and affinity represents the nucleosome-binding affinity score. We defined a low affinity score as a nucleosome-depleted region.

3. Results

3.1. Transcriptome profiles of pheromone-induced yeast

Aymoz *et al.* classified 14 natural pheromone-responsive promoters according to their response times into the early, intermediate, and late stages [18]. The maximum response time of these promoters was mostly concentrated within 10–40 min. However, a dataset of 14 promoters was too small to allow further analysis. In 2000, Roberts *et al.* studied the transcriptional profile of the yeast mating pathway under pheromone treatment using a DNA microarray composed of >97% of known or predicted genes. Their findings summarized the upregulation genes after a 120-min treatment with 50 nM α-factor [7]. Given that

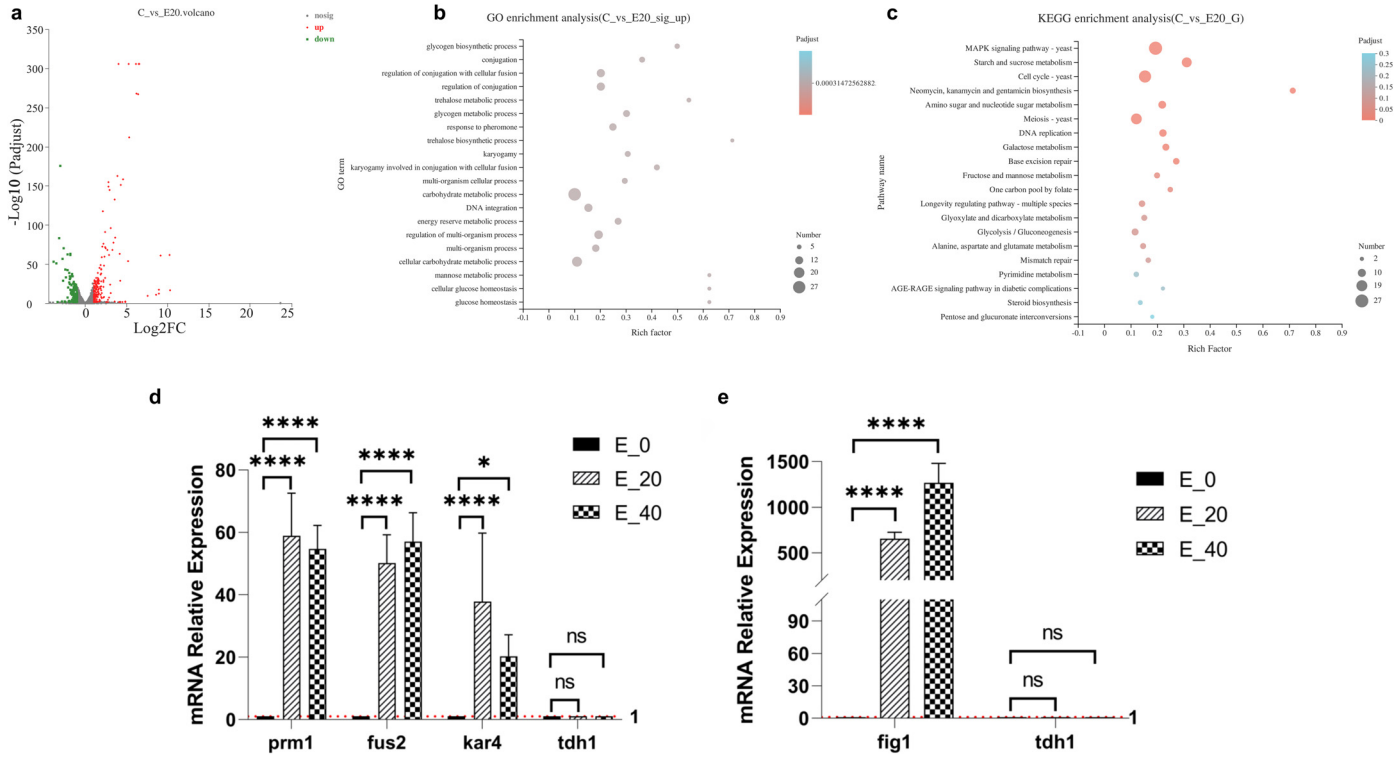

Fig. 1. Transcriptome analysis of *S. cerevisiae* under pheromone treatment based on RNA-Seq. (a) Volcano plot of differential gene expression between control and 20-minute treatment group. (b) Comparisons of Gene Ontology enrichment analysis of significantly upregulated genes between control and 20-minute treatment group. (c) Comparisons of KEGG pathway enrichment of significantly upregulated genes between control and 20-minute treatment group. (d) Transcriptional changes of p*prm1*, p*fus2*, and p*kar4*. (e) Transcriptional changes of p*fig1*, ns: not significant. E_0: control group without α-factor treatment; E_20: experimental group with α-factor treatment for 20 min; E_40: experimental group with α-factor treatment for 40 min.

yeasts use a temporal gradient of pheromones to regulate the timing of mating gene expression, we conducted a transcriptome analysis of yeast BY4741 treated with α-factor for 20 min (early genes) and 40 min (intermediate genes) (NCBI accession number: PRJNA902132). The transcript levels of each gene were then sorted based on the fragments per kilobase of transcripts per million mapped reads (FPKM) values. Upon 5 μM pheromone treatment, 196 genes were significantly upregulated after 20 min (Fig. 1a), and 146 genes were significantly upregulated after 40 min (Fig. S1A). Compared to a 20-minute treatment with pheromones, 40-minute treatment resulted in a significant upregulation of 37 genes and downregulation of 95 genes (Fig. S1D). After screening for promoters associated with mating-specific genes, a pheromone-inducible promoter library comprising 206 promoters was obtained, providing a foundation for engineering artificial promoters (Table S1). By searching for the cPRE sequence motif (5′-TGAAAC-3′) and its close relatives in the library, we noted that all these promoters contain a cPRE or ncPREs, underscoring the significance of PREs in bestowing pheromone-inducible promoter functionality. However, their transcription start sites are yet to be discovered. Hence, the promoter region in this study was defined from the end of the previous gene to the start codon of this gene, i.e., the position immediately upstream of the ATG site was designated as –1.

According to the gene ontology (GO) enrichment analysis, the expression of genes associated with cellular carbohydrate metabolism was significantly upregulated in the 20-minute treatment compared to the control (Fig. 1b). This indicates that although pheromone treatment causes growth arrest, the central carbon metabolism in the cell remains active, which is suitable for the synthesis of heterologous metabolites. After 40 min of treatment, the expression of genes related to polarized growth increased, suggesting that the cells were undergoing shmooing toward the direction of the highest pheromone concentration (Fig. S1B). Compared to the 20-min treatment, the activity of hydrolytic enzymes that act on O-glycosylated compounds and glycosidic bonds significantly increased after 40 min of treatment (Fig. S1E). These enzymes may be involved in cell wall remodeling, facilitating the formation of prezygotes.

Kyoto Encyclopedia of Genes and Genomes enrichment analysis results showed that after 20 min of pheromone induction, the MAPK signaling pathway was activated and the metabolic levels related to the cell cycle and meiosis were higher, indicating that the expression of certain genes related to the cell cycle was arrested at this stage (Fig. 1c). Starch, sucrose, amino sugars, nucleotide sugars, and galactose metabolism were active. After 40 min of treatment, the activity of the MAPK signaling pathway remained high, whereas the cell cycle was arrested in the G1 phase (Fig. S1c). However, metabolic pathways related to the cell cycle and meiosis were maintained at high levels. Compared to the 20-min treatment, there was an increase in metabolic activity related to alanine, aspartate, glutamate, and pyruvate after 40 min of treatment (Fig. S1f). These compounds enter the yeast carbohydrate metabolism directly or indirectly through several reactions [23,24], indicating that the cells have an active central carbon metabolism network. Consequently, cells under pheromone treatment exhibit a strong potential for the production of biochemicals that may have a burden on cell growth, making them suitable for use as a chassis in metabolic engineering. Moreover, metabolic pathway analysis revealed that early genes were predominantly enriched in starch and sucrose metabolism pathways. We found that cellular glycometabolism was maintained at a high level during the mating process, and the metabolic pathway involved in longevity regulation was active (Fig. S1g). Specifically, there was an increase in the levels of glycogen synthesis and degradation, as well as trehalose synthesis during starch and sucrose metabolism (Fig. S1). Intermediate genes were mainly enriched in RNA degradation; purine metabolism; nucleotide sugar and amino sugar metabolism; and alanine, aspartate,

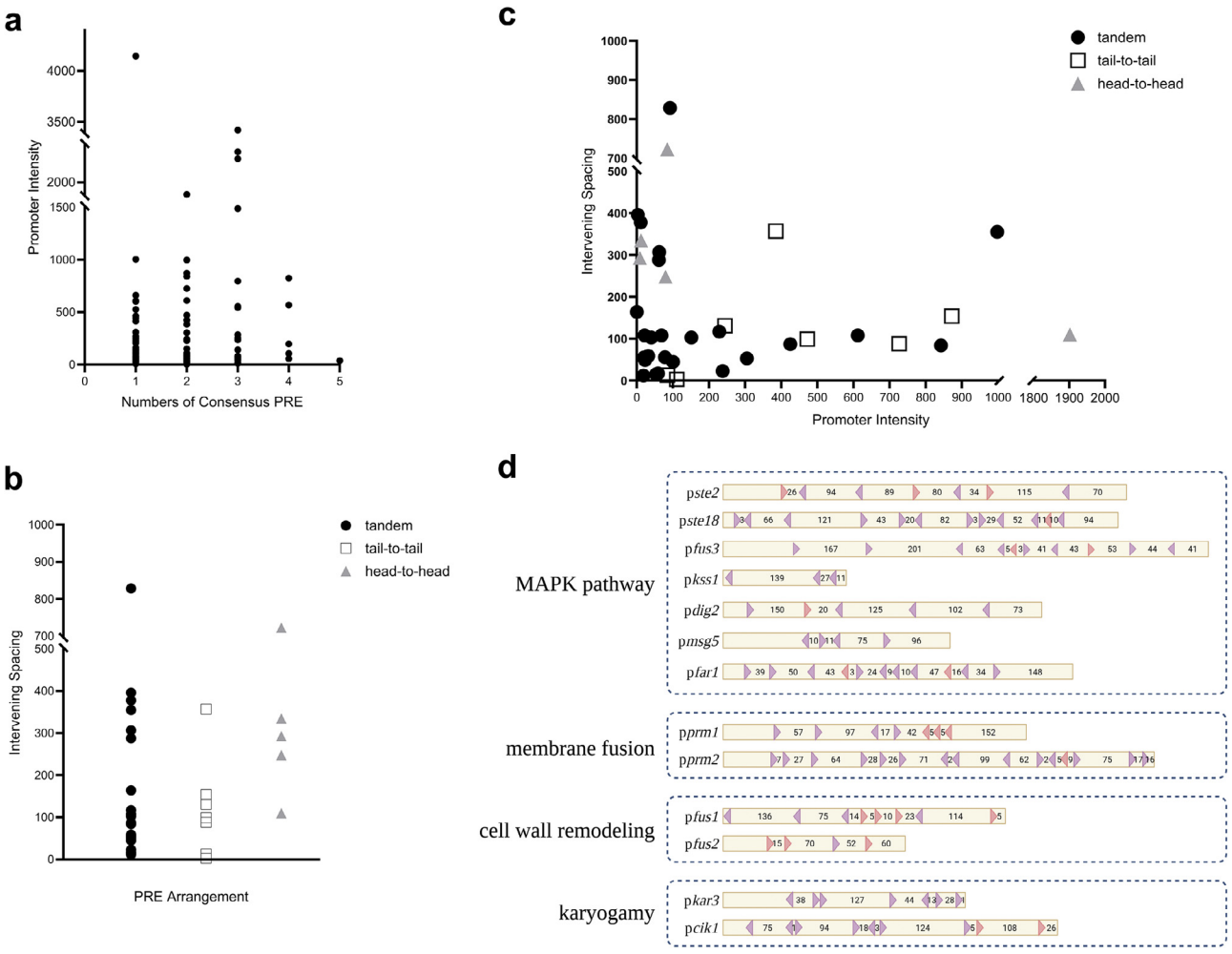

Fig. 2. Architectural analysis of PREs in pheromone-inducible promoters. (a) Correlation between the number of cPREs and promoter intensity. (b) The distribution of distances (spacing) between pairs of cPREs in three possible relative orientations: tandem (both in the same direction), tail-to-tail (facing away from each other), and head-to-head (facing toward each other). (c) Impact of the spacing between two cPRE on promoter intensity within each of the three orientations. (d) Schematic representation of the organization of PREs of the inducible pheromone response genes. Numbers between any two PREs indicate the spacing in nucleotides, whereas the number furthest to the right indicates the distance to ATG. Red arrows: cPREs (5'-TGAAAC-3'); purple arrows: the ncPREs; filled arrow direction: the orientation of the PREs.

and glutamate metabolism (Fig. S1i). These metabolic pathways indicate that the cell undergoes rapid nucleic and amino acid metabolism, providing a material and energy basis for cell fusion. The qPCR results confirmed that the expression of four genes, *prm1, fus2, kar4*, and *fig1*, was upregulated by pheromone induction (Fig. 1d, 1e), consistent with the transcriptome sequencing analysis results.

3.2. Functional diversity of yeast pheromone-induced promoters with the distinct organization of PREs

To understand how PRE architecture affects promoter activity, we used Python to retrieve the copy number, orientation, and intervening spacing of consensus PREs from the 206 promoter sequences in the pheromone-induced promoter library. Among them, approximately 62.6% (129/206) of the promoters contained consensus PREs; hence, we speculated that the absence of consensus PREs may be due to the presence of suboptimal Ste12 binding sites or the need for Ste12 to interact with other unknown *cis*-elements to enhance binding affinity. Of the 129 promoters containing cPREs, 39 contained two PREs, 22 contained three PREs, six contained four PREs, and only one had five PREs. The correlation between the strength of pheromone-induced promoters and the number of cPREs was not distinctly evident (Fig. 2a). However, the promoters containing three cPREs had a higher proportion in the high-activity region than those with any other numbers of cPREs. In addition, several bidirectional promoters with varying activities were identified (Table S1). For example, the complementary sequence of the *prm1* promoter regulated the expression of the *erg4* gene; the same was observed for the *pste2* and *gyp8* promoters.

To explore the relationship between the intervening spacing of the PREs and promoter strength [25], we selected natural pheromone-induced promoters containing two PREs. We visualized the relationship between PRE intervention spacing and promoter strength in three different orientations (tandem, tail-to-tail, and head-to-head) (Figs. 2b and 2c). Our analysis revealed that among the 39 promoters, over two-thirds (27/39) were in the tandem orientation, with intervening spacings mostly under 170 nucleotides and a few over 280 nucleotides (Table S1). However, promoters with PREs in the tandem orientation with intervening spacing between 170–280 nucleotides were not observed. Moreover, no regularity was observed in the tail-to-tail or head-to-head configurations. We also plotted the PRE distribution of typical promoters with different functions in the cell fusion processes (Fig. 2d), providing a basis for downstream PRE-based promoter engineering. Nevertheless, the relationship between copy number, PRE orientation, and promoter activity requires further elucidation. Therefore, it is necessary to estab-

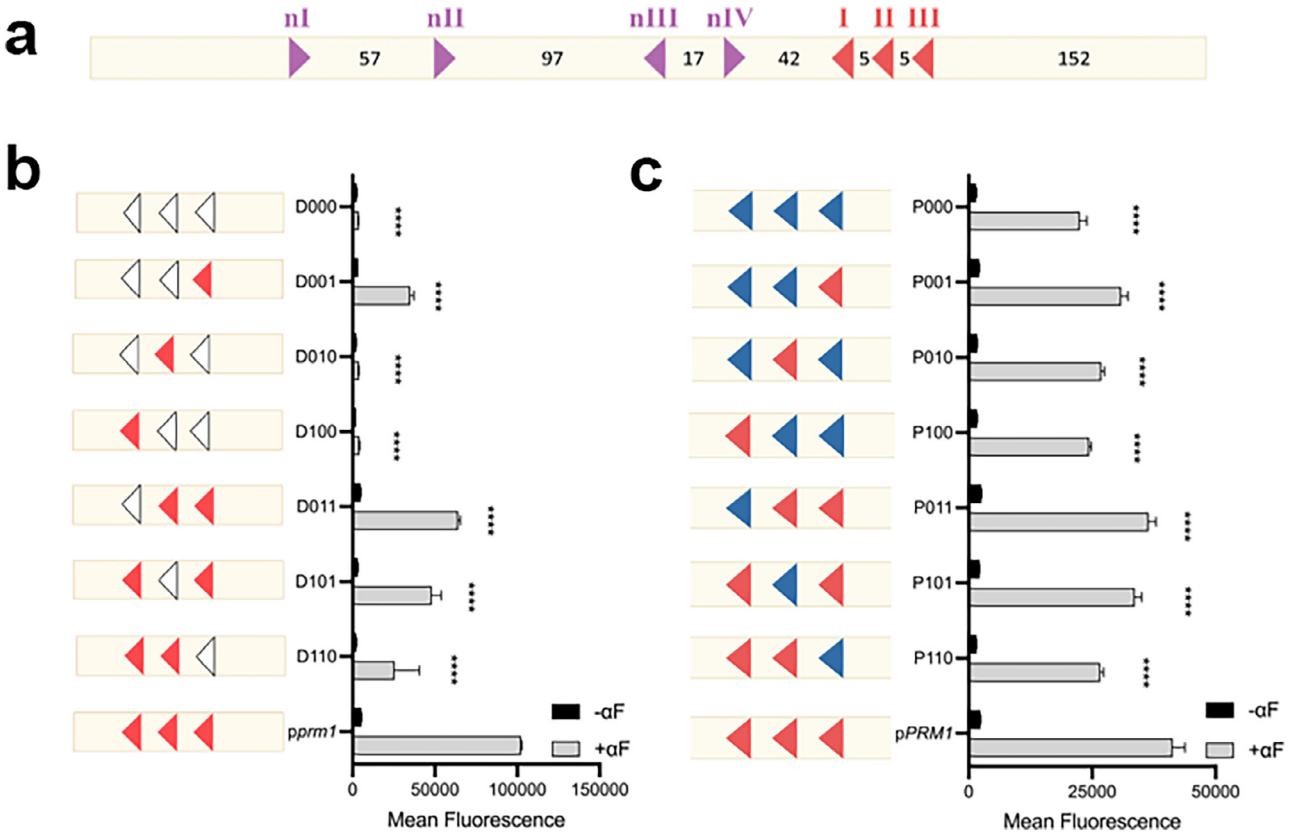

Fig. 3. Contributions of three cPREs in p*PRM1*. (a) Schematic representation of the PRE organization in the wild-type p*PRM1*. Numbers indicate the number of intervening nucleotides between PREs. (b) The impact of PRE deletions on the basal and induced expression levels of p*PRM1*. (c) Comparison of the basal and induced expression levels of artificial promoters with targeted PRE inactivation. The left panel illustrates the corresponding modification scheme of the cPRE in promoters. Purple arrows: the original ncPREs in p*PRM1*; red arrows: cPREs (5'-TGAAAC-3'); blue arrows: inactivated PREs carrying the ncPRE with 5'-TTAAAC-3'; hollow arrows: mutant with PRE knockout. The unit for 'Mean Fluorescence' on the x-axis is in arbitrary units (a.u.). **** corresponds to a p-value < 0.0001; ns indicates non-significance.

lish a mathematical model based on the PRE architecture to predict promoter strength [22].

The relative contribution of three closely spaced cPREs to the expression of p*prm1* cPREs often showed dispersed and random arrangements in many pheromone-inducible promoters (Table S1). In contrast, p*PRM1* contains a proximal PRE locus with three tandem cPREs (5′-AGTAT-3′) oriented opposite to the direction of transcription and interspaced in 5-nt interval, and these PREs were designated as I, II, and III (Fig. 3a). Three PREs in the *PRM1* promoter are required for the Ste12-mediated expression of *PRM1* [26]. Together, these constitute a 28-bp enhancer fragment that activates gene expression from the promoter of the *PRM1* gene. To understand the interplay among the three p*PRM1* cPREs in the activation of pheromone-responsive gene expression, seven mutated promoters (D110 through D000) were generated based on the wild-type promoter, carrying a deletion of a single, double, or all three PREs in the wild-type p*PRM1* (Fig. 3b). The contribution of these enhancer mutants to the promoter activity of *PRM1* were investigated by measuring the fluorescence intensity of GFP. The results showed that the mutant in which all three PREs were deleted from the enhancer (D000) exhibited a residual activity of 3.61% relative to that of the wild-type in the fluorescence assay, indicating that these cPREs play a primary role in the inducibility of the pheromone-induced promoter. As there are four ncPREs located upstream of the cPREs on the *PRM1* promoter, these results suggest that these ncPREs do not activate the basal promoter of *PRM1* (Fig. 3b). Furthermore, PRE deletion analysis suggested that the three cPREs in p*PRM1* may have distinct roles in conferring basal and pheromone-responsive expression. Specifically, the mutation at site III (D110) reduced basal and induced expression by 55.8% and 75.1%, respectively, compared to the wild-type, indicating that it represents the most crucial PRE on p*PRM1* for endowing pheromone inducibility. Consistent with these results, the mutant promoter retaining only PRE site III (D001) conferred 34.2% of the full level of pheromone-inducing activity, whereas mutants retaining either PRE site I (D100) or site II (D010) completely eliminated the response to pheromones.

Because PRE site III in the enhancer is the most proximal site relative to the core promoter, its deletion would change the positions of the remaining PREs relative to the core promoter. To investigate whether the changes in promoter activity stems from the alterations of the relative positions of retaining PREs in the promoter, we constructed similar promoter mutants in the context of the full length promoter by inactivating each of the cPREs by individually converting them to 5′-TTAAAC-3′, an ncPRE that does not facilitate the pheromone-responsive expression, as reported previously [11]. Notably, the change of all three cPREs into ncPREs (P000) yielded only a 45.5% reduction in reporter gene activity, in contrast to the complete loss of activation by D000 (Fig. 2b, 2c), the corresponding motif deletion mutant. Furthermore, mutations in either one or two of these PREs resulted in gene expression levels between the wild-type promoter and P000, all of which showed higher reporter gene activity than the corresponding PRE deletion promoters (Fig. 2c). These results indicate that even though the ncPRE exhibited no apparent affinity for Ste12 *in vitro*, it could still be active *in vivo*. Our results also demonstrated that PRE site III functions not only in pheromone-inducible expression, but also in basal expression, as the levels of basal and inducible expression from the promoter decreased by 33.5% and 35.5%, respectively, compared to those of the wild-type (Fig. 3c, P110).

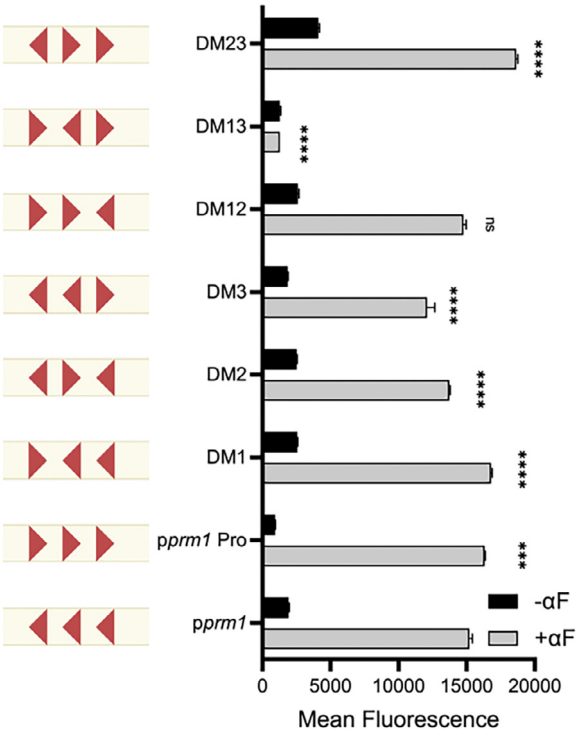

Fig. 4. Comparison of the basal and induced expression levels of artificial promoters based on cPRE orientation modification. The left diagram illustrates the modification scheme of PREs in the promoter. Red arrows represent cPREs, and the arrow direction indicates the orientation of the cPREs. The unit for 'Mean Fluorescence' on the x-axis is in arbitrary units (a.u.). **** corresponds to a p-value < 0.0001; *** to a p-value < 0.001; ns indicates non-significance.

3.3. Influence of element orientations in a short tandem PRE array on promoter activity

The closely spaced PREs in *pPRM1* may be combined in different orientations as enhancer elements; however, the significance of distinct arrangements in promoter activity remains to be elucidated. The orientations of the three tandem PREs in the *PRM1* core enhancer changed individually in all possible combinations, yielding seven mutated promoters (Fig. 4). Reporter gene assays revealed that the inducible expression of p*PRM1* Pro, a promoter in which all three PREs are arranged in the forward orientation, increased by 7.4%, whereas its basal expression level decreased by 50.7% compared to wild-type p*PRM1*. These results indicate that altering the orientation of PREs simultaneously expands the dynamic range of the promoter by increasing inducible expression levels and reducing leakage levels. PREs with the same orientation may endow promoters with a greater dynamic range, making promoter expression closer to an "on/off"switch, which lays the foundation for efficient artificial promoters.

The remaining six variants of p*PRM1*, designated DM1, DM2, DM3, DM12, DM13, and DM23, were also assayed, and the following results were obtained (Fig. 4). First, inducible activity increased for DM1 and DM23 (10.5% and 22.6%, respectively, compared with p*PRM1*). Second, DM2, DM3, and DM13 displayed decreased expression levels, among which a substantial reduction in inducible activity was observed in DM13, which retained only 8.4% of the wild-type level. Similarly, Su *et al.* inverted one of the two cPREs in p*FUS1*, originally separated by three nucleotides in a tandem configuration, creating a "head-to-head" orientation that completely blocked the response to the pheromone. Surprisingly, two cPREs spaced 40 nucleotides apart in a "head-to-head" arrangement generated significant pheromone responses [11]. Inspired by this, a plausible explanation for this phenomenon is that structural constraints of Ste12 might lead to inefficient interactions among its oligomers in the head-to-head arrangement of closely spaced PREs, thereby hindering effective gene expression.

3.4. PRE multiplication expands the dynamic range of the promoter

To test how the copy number of PREs in a promoter affects the level of pheromone-inducible expression, a segment of three PREs was duplicated, yielding p*PRM1* Ultra, which contains six tandem copies of reversely oriented PREs (Fig. 5a). Compared to the wild-type p*PRM1*, p*PRM1* Ultra showed a lower level of basal expression (a decrease of 43.2%), but a higher level of pheromone-induced expression (an increase of 37.8%). These results indicate that PRE multiplication not only synergistically enhanced the pheromone inducibility of the promoters, but also prevented their leakage.

Given that the binding of transcription factors to the promoter is influenced by the positioning of nucleosomes on the DNA [18], we used the NuPoP algorithm (https://bioconductor.org/packages/NuPoP/) to predict the nucleosome structure of the p*PRM1* promoter region. We found that the PRE trimer of p*PRM1* is located in a nucleosome-unfavorable region with a lower affinity for nucleosomes, which is conducive to transcription by avoiding nucleosome interference and can also be regulated by pheromones. Hence, we defined the region from –280 to –101 bp upstream of the p*PRM1* gene start codon, which includes two nucleosome-unfavorable regions, as UAS_{prm1} (Fig. 5b). To assess the feasibility of using UAS_{prm1} as an inducible element, we constructed a synthetic promoter UAS_{prm1}-p*TEF2* by placing UAS_{prm1} upstream of p*TEF2,* a strong constitutive promoter. The results showed that UAS_{prm1} conferred p*TEF2* pheromone inducibility, leading to a 57.78% increase in UAS_{prm1}-p*TEF2* expression upon pheromone induction (Fig. 5c).

Next, we evaluated the effects of UAS_{prm1} on the expression of the core promoters p*AGA1*, p*PRM1*, p*FIG1*, and p*FUS2,* all of which belong to the cPRE-dispersed promoter category. Our findings revealed that UAS_{prm1} expands the dynamic range of promoters as an efficient pheromone-inducible element. Specifically, the promoters in tandem with UAS_{prm1} exhibited an expanded dynamic range of promoter activity by decreasing basal expression levels and improving inducible activity (Fig. 5d). For example, the enhancer decreased the basal expression of p*FUS2* and p*AGA1* by 65.6% and 35.3%, respectively (Fig. 5d). Furthermore, UAS_{prm1}-p*FIG*1 and UAS_{prm1}-p*FUS2* exhibited activity levels 1.5 and 1.3 times higher than that of the wild-type, respectively (Table 1). However, no change in the inducible expression of p*AGA1*, a promoter exhibiting strong pheromone-inducible activity, was observed when combined with UAS_{prm1} (Table 1). Furthermore, the induction effect of UAS_{prm1}-p*PRM1* was not as significant (12.6%) as that of p*PRM1* Ultra (37.8%). We speculated that this difference could be attributed to the increased distance between the Ste12 interaction sites, which could hinder Ste12 polymerization. Together, these results indicate that adding multiple copies of PRE upstream of the promoters can significantly affect their expression at the basal and pheromone-induced levels.

3.5. PREs and ncPREs may form enhancer-enhancer hubs to synergistically confer pheromone-responsive gene expression

The native p*PRM1* promoter contains three proximal cPRE motifs and four distal ncPRE motifs. Because ncPREs have a low affinity for Ste12, we were interested to determine the effect of mutating them into cPREs and the inducible activity of the promoter. Promoters with one or more distal ncPREs converted into cPREs were constructed and assayed for their promoter activity. Among the 15 mutations (Table 1), the induction activities of five mutant promoters, CM2, CM23, CM123, CM234, and CM1234, were significantly improved (Fig. 6). Restoration of the cPRE at the second ncPRE site was common among the five mutant promoters, and four of them restored the third ncPRE site, indicating a crucial role for these two positions in enhancing the induction strength

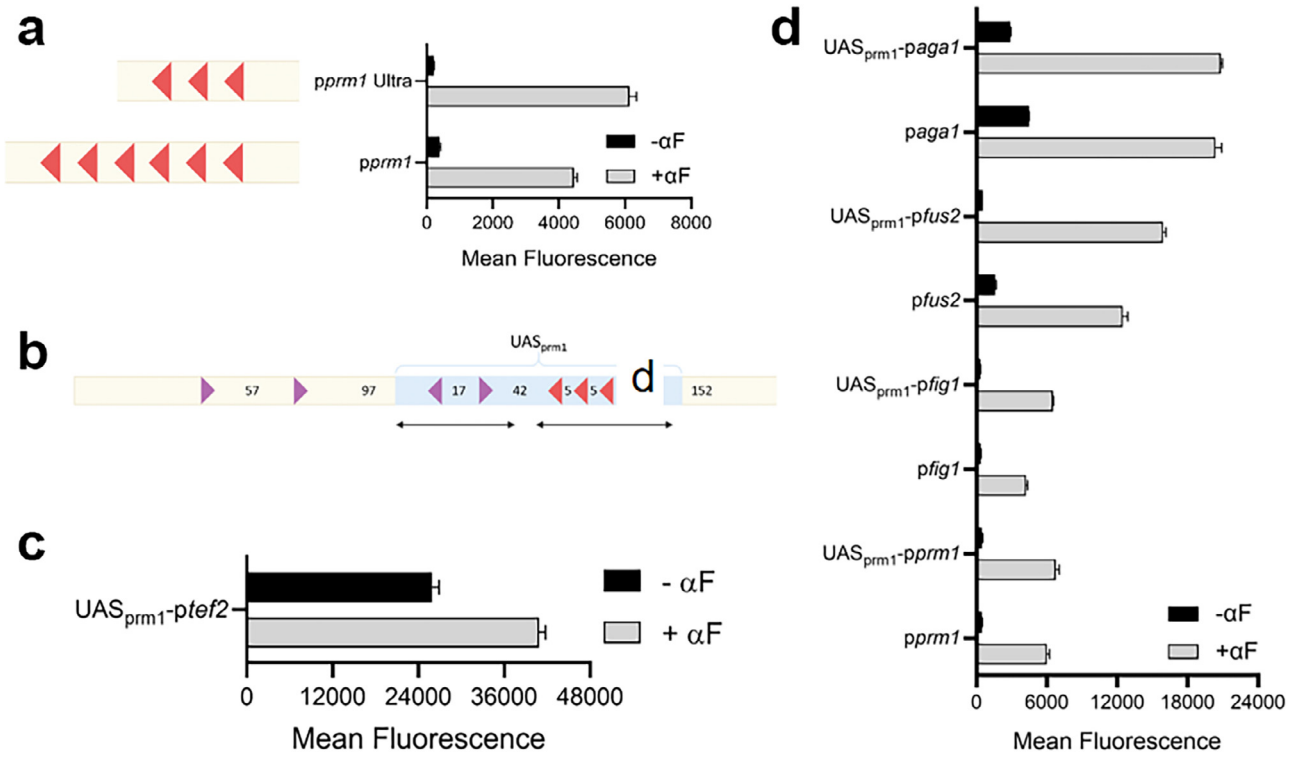

Fig. 5. The impact of copy number increase on promoter activity. (a) Comparison of the basal and induced expression levels of p*PRM1* Ultra and p*PRM1*. The left diagram illustrates the arrangement of PREs in the promoters. (b) Schematic diagram of p*PRM1*, where the blue region indicates the UAS_{prm1} region. Red arrows: cPRE; purple arrows: ncPRE; bidirectional arrows: nucleosome-disfavoring region; numbers: the number of intervening nucleotides. (c) Promoter activity of UAS_{prm1}-p*TEF2* under pheromone treatment. (d) The impact of UAS_{prm1} on the basal and induced expression levels of p*AGA1*, p*FUS2*, p*FIG1*, and p*PRM1*.

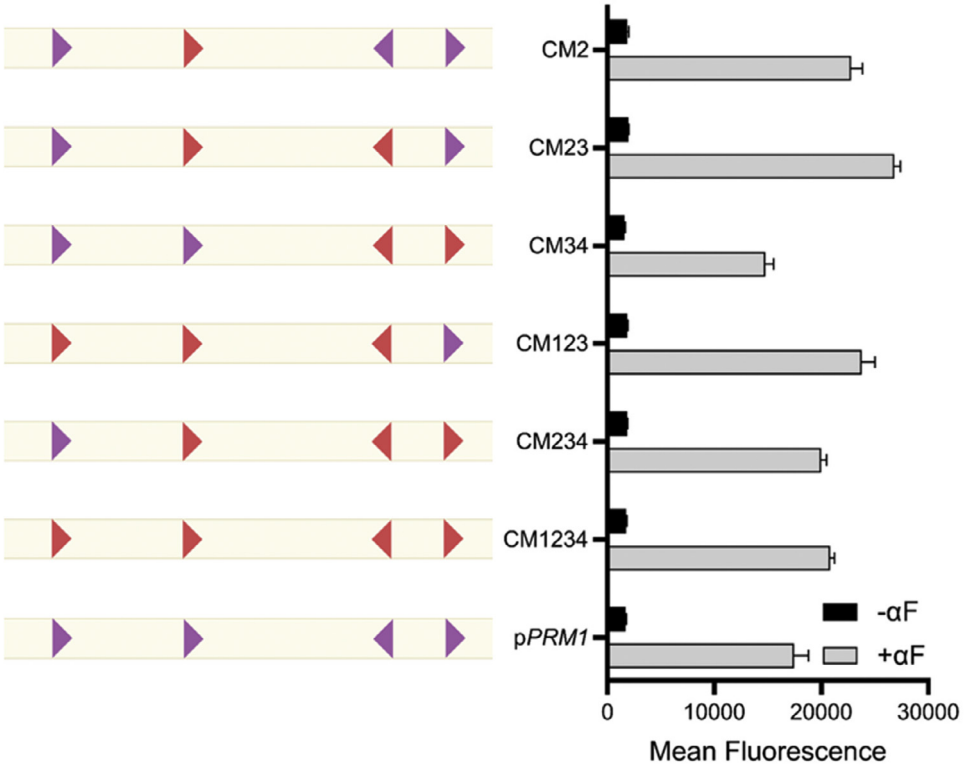

Fig. 6. The effect of mutating ncPREs into cPREs on basal and induced expression levels. The left diagram illustrates the modifications of ncPREs in the promoters. Red arrows: cPREs; purple arrows: ncPREs. The arrow direction represents the orientation of the PREs.

Table 1
Activities of synthetic promoters based on pheromone response element (PRE) modification.

	Promoter	-αF	+αF	+/-αF[a]
Differential contribution of each PRE (deletion)	pPRM1	/	/	18.8
	D011	↓9.6%	↓37.4%	13.0
	D101	↓39.5%	↓53.0%	14.6
	D110	↓55.8%	↓75.1%	10.6
	D100	↓59.3%	↓95.9%	1.9
	D010	↓57.3%	↓96.2%	1.7
	D001	↓35.5%	↓65.8%	10.0
	D000	↓52.0%	↓96.4%	1.4
Differential contribution of each PRE (site-specific inactivation)	pPRM1	/	/	17.1
	P011	↓6.7%	↓11.8%	14.2
	P101	↓8.2%	↓18.5%	15.1
	P110	↓33.5%	↓35.5%	16.6
	P100	↓29.4%	↓40.9%	14.3
	P010	↓27.8%	↓35.0%	15.4
	P001	↓10.8%	↓25.3%	14.3
	P000	↓37.7%	↓45.5%	15.0
Alternations in PRE orientation	pPRM1	/	/	7.9
	DM1	↑34.0%	↑10.5%	6.5
	DM2	↑30.6%	↓9.7%	5.5
	DM3	NS	↓20.5%	6.5
	DM12	↑35.7%	NS	5.7
	DM13	↓33.4%	↓91.6%	1.0
	DM23	↑114.0%	↑22.6%	4.5
	pPRM1 Pro	↓50.7%	↑7.4%	17.2
Alternations in PRE copy numbers	pPRM1	/	/	11.7
	pPRM1 Ultra	↓43.2%	↑37.8%	28.3
	pPRM1	/	/	12.4
	UASprm1-pPRM1	NS	↑12.6%	13.9
	pFIG1	/	/	11.5
	UASprm1-pFIG1	↓11.0%	↑53.9%	19.8
	pFUS2	/	/	7.7
	UASprm1-pFUS2	↓65.6%	↑27.5%	28.7
	pAGA1	/	/	4.5
	UASprm1-pAGA1	↓35.3%	NS	7.2
Synergy between cPREs and ncPREs	pPRM1	/	/	10.2
	CM1	NS	NS	9.9
	CM2	NS	↑30.6%	12.2
	CM3	↓15.5%	NS	11.2
	CM4	↓9.4%	NS	10.6
	CM12	NS	NS	10.2
	CM13	NS	NS	10.3
	CM14	NS	NS	10.0
	CM23	↑14.9%	↑53.6%	13.6
	CM24	NS	NS	11.2
	CM34	NS	↓15.4%	9.3
	CM123	↑8.7%	↑36.3%	12.7
	CM124	NS	NS	9.4
	CM134	NS	NS	10.0
	CM234	NS	↑14.6%	10.8
	CM1234	NS	↑19.3%	12.0

[a] Ratio of the mean fluorescence in MATa cells treated with α-factor to that in untreated cells.

of the *PRM1* promoter. The highest inductivity was observed for CM23 (53.6%), highlighting the importance of these two sites.

Moreover, the impact of ncPRE mutations on the basal expression levels of promoters CM23 and CM123 was consistent with their effect on the induced expression levels, as shown in Table 1. Notably, only the CM34 mutant showed a significant decrease in induced activity, with a decrease of 15.4% compared with that of the wild-type p*PRM1*. By comparing the decrease in induced activity between CM1234 and CM123 and between CM234 and CM23, we inferred that the mutation at site 4 may have a decreasing effect on the induced activity of the *PRM1* promoter when combined with other site mutations. Next, we mutated the unique ncPRE of p*FUS2* into a cPRE, which was defined as p*FUS2*-fgs. Contrary to our expectations, the strength of the inducible p*FUS2*-fgs decreased by 22% (Fig. S2). These results showed that the correlation between the number of PRE copies and promoter activity did not show a positive linear correlation and that promoter activity was also influenced by the overall PRE configuration, such as its position and orientation. Together, these factors constrain the activation of PREs to the expression of pheromone-responsive genes, and these constraints could reflect the logic of interactions between PREs and Ste12, as well as their interaction with the basal transcriptional machinery.

4. Discussion

The pheromone response pathway in *S. cerevisiae* has emerged as a critical model for elucidating the mechanisms underlying inducible promoters. However, many unresolved questions remain regarding the mechanisms involved in their regulation [19,27], such as the molecular mechanisms that control their activity by upstream MAPKs, how they tune basal expression and transcriptional activation, and the mechanism by which they regulate the interaction between PREs and Ste12. Recent studies on genome organization have revealed that the dynamic reconnection of promoter-enhancer hubs is closely associated with increased gene expression and plays a role in determining cell fate [28,29]. To improve our understanding of yeast promoter-enhancer hub regulation and functionality, it is essential to systematically perturb their constituent components and assess their effects on gene expression [30]. This study explored the correlation between the *in vivo* responsiveness of multiple PREs to pheromones and their spatial orientation by investigating the impact of PRE copy number and orientation on promoter strength. This study sheds light on the transcriptional mechanism of pheromone-inducible promoters, enabling the rational engineering of artificial promoters with a wide dynamic range and further applications in other fields, such as metabolic engineering of toxic products and more sensitive biosensors [5].

4.1. Basic model of PRE-mediated Ste12 oligomerization interaction

Given that Ste12 requires oligomerization to activate pheromone responses *in vivo* [11,12,19,20], we proposed a model for regulating the pheromone-induced promoter. As a eukaryotic signal-responsive transcription factor [31], Ste12 has the following residue annotations: a DNA-binding domain, activation and multimerization domains, and inhibitor protein-binding domains. The first 215 residues of the N-terminal domain are responsible for recognizing and binding to PREs, and residues 262–594, which have polymerization sites, allow the effective conservation of pheromone-induced activity [32]. Previously, Su *et al.* [11] proposed a relevant model that assumed that the connection between the C- and N-termini of Ste12 is flexible and rotatable. With the exception of the “head-to-head” configuration at close distances, which cannot be transcribed due to the steric hindrance caused by the asymmetry of the N-terminus of Ste12, all other configurations can activate transcription due to the flexibility of DNA and Ste12. However, their model fails to account for all their experimental results, as evidenced by the fact that two PREs with the same 40-nucleotide spacing barely activated p*GAL1* in a tandem configuration, whereas strong activation was observed for the head-to-head and tail-to-tail configurations [11]. In contrast, we believe that the spatial structure of the Ste12 protein is noncentrosymmetric and rigid [11].

Based on their model and our experimental results, we hypothesized a fundamental model using two simplified PREs as examples, illustrating the recruitment of Ste12 and the promotion of its oligomerization by PREs with different configurations and distance arrangements (Fig. 7). When the two PREs were in “close” proximity, only the tandem is capable of recruiting and promoting Ste12 oligomerization (Fig. 7c). In the head-to-head configuration of the PREs, Ste12 recruitment can be hindered by steric effects, resulting in the failure of Ste12 to bind to the PRE (Fig. 7a). On the other hand, the tail-to-tail configuration is also not conducive for Ste12 oligomerization and activation (Fig. 7B). When the distance between two PREs is sufficiently large, DNA can achieve

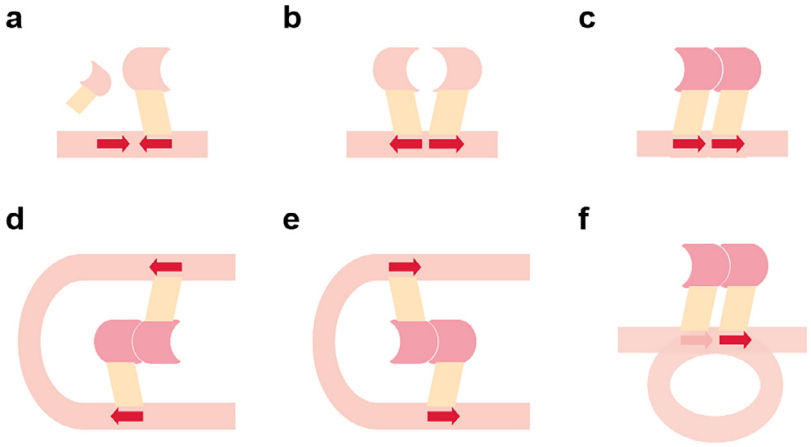

Fig. 7. The configuration and distance of two PREs affect the interaction with Ste12. When the two PREs are in close proximity (a, b, c), the "head-to-head" (a) and "tail-to-tail" configuration (b) are ineffective, whereas the tandem configuration (c) is effective. When the two PREs are at a distance (d, e, f), the "head-to-head" configuration (d) and "tail-to-tail" configuration (e) function through DNA bending, while the tandem configuration (f) functions through DNA looping. Red arrows: cPREs; arrow direction: the orientation of the cPREs; yellow diamond: DNA-binding domain of Ste12; light pink arc: unoligomerized Ste12; dark pink arc: oligomerized Ste12.

tandem interactions to promote Ste12 oligomerization through bending or looping. In addition to distance, the choice of bending or looping the DNA also depends on the orientation of the PREs. When two “distantly” spaced PREs are oriented oppositely, the DNA tends to bend because it utilizes less energy to meet the oligomerization needs of Ste12 (Fig. 7d, 7e). When the orientations of the PREs are the same and the distance between them is greater than the minimum looping distance, DNA prefers to form a tandem structure through looping (Fig. 7f). The recruited Ste12 oligomer can then further recruit potential mediator proteins that indirectly affect RNA polymerase, ultimately leading to transcriptional activation.

However, we were unable to define a clear numerical boundary for “near” and “far,” as this has not been studied. We consider 5 bp to be within the “near” range, which should have a maximum value; while “far” has a minimum value, which is the smallest number of bases or the optimal number of bases that allow DNA to bend. Owing to the structural similarities between pheromone-induced and galactose-inducible promoters [33], the conclusion of our study has important implications for the investigation of eukaryotic regulatory systems other than pheromone-inducible expression. This will be highly significant for studying how multiple PRE interactions mediate pheromone responses and understanding Ste12-PRE interactions *in vivo*.

Data availability statement

The raw data of RNA-seq with a sequencing depth of 2 billion data volumes for each sample had been uploaded to NCBI gene bank under the accession number PRJNA902132.

Declaration of competing interest

The authors declare that they have no known competing financial interests or personal relationships that could have appeared to influence the work reported in this paper.

CRediT authorship contribution statement

Yiqing Zhang: Writing – original draft, Visualization, Project administration, Methodology, Investigation, Formal analysis, Data curation, Conceptualization. **Yinfeng Wei:** Writing – review & editing, Methodology, Formal analysis. **Yuxin Huang:** Methodology, Investigation. **Chenyu Wang:** Methodology, Investigation, Data curation. **Tao Wang:** Methodology, Investigation, Funding acquisition. **Yujiao Wang:** Methodology, Investigation. **Yingxuan Qi:** Methodology, Investigation. **Guannan Liu:** Writing – review & editing, Writing – original draft, Supervision, Project administration, Methodology, Investigation, Funding acquisition, Data curation, Conceptualization.

Acknowledgements

This study was supported by the Jiangsu Basic Research Center for Synthetic Biology (BK20233003), Jiangsu Synergetic Innovation Center for Advanced Bio-Manufacture (XTD2214), National Natural Science Foundation of China (21808109), Natural Science Foundation of Jiangsu Province (BK20180703), Natural Science Foundation of Tianjin Municipality (18JCQNJC10200). T.W was supported by the National Students’ Platform for Innovation and Entrepreneurship Training Program (202410291018Z).

Supplementary materials

Supplementary material associated with this article can be found, in the online version, at doi:10.1016/j.engmic.2025.100249.

References

[1] C.S. Lee, J.E. Haber, Mating-type Gene Switching in Saccharomyces cerevisiae, Microbiol Spectr 3 (2015) MDNA3-0013-2014.
[2] M.J. Winters, P.M. Pryciak, MAPK modulation of yeast pheromone signaling output and the role of phosphorylation sites in the scaffold protein Ste5, Mol Biol Cell 30 (2019) 1037–1049.
[3] Y. Li, J. Roberts, Z. AkhavanAghdam, N. Hao, Mitogen-activated protein kinase (MAPK) dynamics determine cell fate in the yeast mating response, J Biol Chem 292 (2017) 20354–20361.
[4] I. Herskowitz, MAP kinase pathways in yeast: for mating and more, Cell 80 (1995) 187–197.
[5] Y. Liu, Y. Huang, R. Lu, F. Xin, G. Liu, Synthetic biology applications of the yeast mating signal pathway, Trends Biotechnol 40 (2022) 620–631.
[6] L. Bardwell, A walk-through of the yeast mating pheromone response pathway, Peptides 26 (2005) 339–350.
[7] C.J. Roberts, B. Nelson, M.J. Marton, R. Stoughton, M.R. Meyer, H.A. Bennett, et al., Signaling and circuitry of multiple MAPK pathways revealed by a matrix of global gene expression profiles, Science 287 (2000) 873–880.
[8] J.W. Dolan, C. Kirkman, S. Fields, The yeast STE12 protein binds to the DNA sequence mediating pheromone induction, Proc Natl Acad Sci USA 86 (1989) 5703–5707.
[9] P. Sengupta, B.H. Cochran, The PRE and PQ box are functionally distinct yeast pheromone response elements, Mol Cell Biol 10 (1990) 6809–6812.
[10] S.W. Van Arsdell, G.L. Stetler, J. Thorner, The yeast repeated element sigma contains a hormone-inducible promoter, Mol Cell Biol 7 (1987) 749–759.
[11] T.C. Su, E. Tamarkina, I. Sadowski, Organizational constraints on Ste12 cis-elements for a pheromone response in Saccharomyces cerevisiae, FEBS J 277 (2010) 3235–3248.
[12] D.C. Hagen, G. McCaffrey, G.F. Sprague Jr., Pheromone response elements are necessary and sufficient for basal and pheromone-induced transcription of the FUS1 gene of Saccharomyces cerevisiae, Mol Cell Biol 11 (1991) 2952–2961.
[13] J. Trueheart, J.D. Boeke, G.R. Fink, Two genes required for cell fusion during yeast conjugation: evidence for a pheromone-induced surface protein, Mol Cell Biol 7 (1987) 2316–2328.
[14] B. Errede, G. Ammerer, STE12, a protein involved in cell-type-specific transcription and signal transduction in yeast, is part of protein-DNA complexes, Genes Dev 3 (1989) 1349–1361.
[15] S. Chou, S. Lane, H. Liu, Regulation of mating and filamentation genes by two distinct Ste12 complexes in Saccharomyces cerevisiae, Mol Cell Biol 26 (2006) 4794–4805.

[16] W. Zheng, H. Zhao, E. Mancera, L.M. Steinmetz, M. Snyder, Genetic analysis of variation in transcription factor binding in yeast, Nature 464 (2010) 1187–1191.
[17] S.W. Van Arsdell, Hormonal regulation of gene expression in yeast, in: In *Transcriptional Control Mechanisms*, Alan R. Liss inc., 1987, pp. 325–332.
[18] D. Aymoz, C. Sole, J.J. Pierre, M. Schmitt, E. de Nadal, F. Posas, et al., Timing of gene expression in a cell-fate decision system, Mol Syst Biol 14 (2018) e8024.
[19] M.W. Dorrity, J.T. Cuperus, J.A. Carlisle, S. Fields, C. Queitsch, Preferences in a trait decision determined by transcription factor variants, Proc Natl Acad Sci USA 115 (2018) E7997–E8006.
[20] Y.L. Yuan, S. Fields, Properties of the DNA-binding domain of the Saccharomyces cerevisiae STE12 protein, Mol Cell Biol 11 (1991) 5910–5918.
[21] Z. Che, X. Cao, G. Chen, Z. Liang, An effective combination of codon optimization, gene dosage, and process optimization for high-level production of fibrinolytic enzyme in Komagataella phaffii (Pichia pastoris), BMC Biotechnol 20 (2020) 63.
[22] L. Xi, Y. Fondufe-Mittendorf, L. Xia, J. Flatow, J. Widom, J.P. Wang, Predicting nucleosome positioning using a duration Hidden Markov Model, BMC Bioinformatics 11 (2010) 346.
[23] J. Lian, S. Mishra, H. Zhao, Recent advances in metabolic engineering of Saccharomyces cerevisiae: New tools and their applications, Metab Eng 50 (2018) 85–108.
[24] L. Yang, C. Jia, B. Xie, M. Chen, X. Cheng, X. Chen, et al., Lighting up Pyruvate Metabolism in Saccharomyces cerevisiae by a Genetically Encoded Fluorescent Biosensor, J Agric Food Chem 72 (2024) 1651–1659.
[25] S. Li, L. Ma, W. Fu, R. Su, Y. Zhao, Y. Deng, Programmable Synthetic Upstream Activating Sequence Library for Fine-Tuning Gene Expression Levels in Saccharomyces cerevisiae, ACS Synth Biol 11 (2022) 1228–1239.
[26] T. Hofken, Ecm22 and Upc2 regulate yeast mating through control of expression of the mating genes PRM1 and PRM4, Biochem Biophys Res Commun 493 (2017) 1485–1490.
[27] L. Mahendrawada, L. Warfield, R. Donczew, S. Hahn, Low overlap of transcription factor DNA binding and regulatory targets, Nature 642 (2025) 796–804.
[28] J. Zhao, R.B. Faryabi, Spatial promoter-enhancer hubs in cancer: organization, regulation, and function, Trends Cancer 9 (2023) 1069–1084.
[29] I.K. Nolis, D.J. McKay, E. Mantouvalou, S. Lomvardas, M. Merika, D. Thanos, Transcription factors mediate long-range enhancer-promoter interactions, Proc Natl Acad Sci U S A 106 (2009) 20222–20227.
[30] D.C. Di Giammartino, A. Polyzos, E. Apostolou, Transcription factors: building hubs in the 3D space, Cell Cycle 19 (2020) 2395–2410.
[31] C. Randise-Hinchliff, R. Coukos, V. Sood, M.C. Sumner, S. Zdraljevic, L. Meldi Sholl, et al., Strategies to regulate transcription factor-mediated gene positioning and interchromosomal clustering at the nuclear periphery, J Cell Biol 212 (2016) 633–646.
[32] K.A. Olson, C. Nelson, G. Tai, W. Hung, C. Yong, C. Astell, et al., Two regulators of Ste12p inhibit pheromone-responsive transcription by separate mechanisms, Mol Cell Biol 20 (2000) 4199–4209.
[33] G.L. Elison, Y. Xue, R. Song, M. Acar, Insights into Bidirectional Gene Expression Control Using the Canonical GAL1/GAL10 Promoter, Cell Rep 25 (2018) 737-748 e734.